

Received April 16, 2018; reviewed; accepted May 24, 2018

Three-phase contact line expansion during air bubble attachment to hydrophobic solid surface – experiment and modeling

Pavlina Basarova¹, Katerina Souskova¹, Jan Zawala²

¹ University of Chemistry and Technology, Prague, Czech Republic

² Jerzy Haber Institute of Catalysis and Surface Chemistry Polish Academy of Sciences, Krakow, Poland

Corresponding author: Pavlina.Basarova@vscht.cz (Pavlina Basarova)

Abstract: Kinetics of spreading of the three-phase contact hole (dewetting) formed by an air bubble colliding with hydrophobic solid surface, after rupture of intervening liquid film, was studied both experimentally and numerically. During experiments it was found that evolution of the TPC line diameter with time occurs with characteristic S-shaped trend which, in consequence, causing rather unexpected maxima at the TPC line spreading velocity curves. It was determined that position of this maximum appears after 1-2 ms after TPC hole formation and its position (in respect to time) depends on the bubble diameter. In solution of surface-active substance this maximum was much smoother and longer. By means of complementary numerical calculations the source of maxima existence and differences in their position and shapes were explained. It was concluded that this effect has only hydrodynamic origin, caused by different course of bubble shape pulsations during TPC line formation and spreading, which depends on degree of liquid/gas interface immobilization (fluidity retardation).

Keywords: three-phase contact, bubble, attachment, dewetting, simulations

1. Introduction

The attachment of bubbles onto a solid surface plays a critical role in many industrial applications. The bubble adhesion onto the hydrophobic particle and the stability of the created unit determine the effectiveness of the interaction process. The bubble attachment consists of two terms: (1) the thinning of liquid film to a critical thickness where rupture of the liquid film begins; and (2) the expansion of the three-phase contact line to form a stable wetting perimeter (Nguyen et al., 1997). This perimeter is usually known as the three-phase contact line (TPC line). After the formation of the TPC line its movement can be observed. Historically, literature mentions two main approaches when dealing with the kinetics of the TPC line based either on the hydrodynamic (Huh and Scriven, 1971; Cox, 1986) or molecular-kinetic theories (Yarnold and Mason, 1949; Blake and Haynes, 1969). The presence of surfactants may significantly affect the kinetics of this process (Kosior et al., 2013; Krasowska et al., 2009; Zawala et al., 2015). The TPC line dynamics is influenced by the surfactant adsorption on solid-liquid, solid-gas and liquid-gas interphases and also by the Marangoni flow along the bubble surface due to the changing surfactant concentration (Radulovic et al., 2013). Surfactants also damp significantly the bubble shape oscillations, because they decrease the elasticity of interface (Vobecka et al., 2012).

In case of pure liquids, the liquid phase (after the rupture of the interface film) begins to retreat from the solid surface due to an uneven distribution of the liquid-gas interfacial tension (surface tension gradients). The contact line movement is driven by fluid dynamics, but surface tension and inertial and viscous forces influence the expansion of the TPC line too. The resultant of the forces influences the curvature of the liquid-gas interface and therefore affects the shape of the bubble. At first glance, the bubble adhesion (dewetting process) is similar to the drop spreading (wetting). The spreading process is dominated by the fluid viscous dissipation and the bulk viscous friction is usually the main resistance force for the TPC line contact motion (Ranabothu et al., 2005). Here, the theory solves the equations

governing the fluid dissipation, the continuity and Navier-Stokes equations. In the case of bubble adhesion, we have to consider also additional forces resulting from quite violent bubble shape pulsations. These oscillations were observed experimentally in case of bubbles with mobile surface (Basarova and Souskova, 2018). Immobilization of the bubble surface, e.g. by the addition of a surfactant, results in the suppression of bubble shape oscillations.

In this project, kinetics of the TPC line expansion during bubble collision and rupture at hydrophobic solid surface was studied by means of numerical simulations, both for completely mobile (slip) and fully immobilized (no-slip) liquid/gas interface. The obtained results were compared with experimental data obtained in corresponding conditions. The primary focus was put on explanation of origin of rather unexpected characteristic peaks observed for TPC line velocity vs. time dependence. It was found that position of these peaks depends on bubble radius and liquid/gas interface properties. Thanks to the simulations, the mechanism of this effect was discussed and explanation for surprising trends of the TPC line velocity variations was proposed.

2. Materials and methods

2.1. Experiments

The experimental measurements were performed in a special glass cell (rectangular cross-section, 30 cm height, 8 cm width and 6 cm depth). Single bubbles were created by a bubble generator at the top of a thin capillary with the inner diameter 10 μm (Hubicka et al., 2013). The resulting bubble diameter 0.70 and 0.85 mm was adjusted by control of the bubble growing time. After detaching from the capillary, the bubble rose through the liquid to the horizontal solid plate. Silanized glass was used as a model hydrophobic surface (Basarova and Souskova, 2018). The distance between the capillary tip and the solid surface was 20 cm, i.e. was far enough for the rising bubble to reach its terminal velocity. The phenomena occurring during the bubble-solid surface interactions, i.e. the bubble motion before and after the collision with the solid particle as well as during the adhesion, was recorded using a high-speed digital camera Photron FastCam SA1.1 (16000 fps, resolution of 1024×1024 pixels, calibration 2.8 μm per pixel) with a Navitar macro objective. At least five video sequences were captured for every size of the bubble. The image analysis was done using the NIS-Elements Advanced Research software. All the sequences were qualitatively observed with regard to possible bouncing, bubble shape deformation and the symmetry of three-phase contact line expansion. The development of the diameter of TPC line (d_{TPC}) over time and variations in the vertical position of the bubble bottom apex (y_{bottom}) were evaluated for each sequence. The bubble diameter (d_b) and the final equilibrium contact angle (θ_b) were measured for every sequence as well. The velocity of TPC expansion (U_{TPC}) was calculated as:

$$U_{TPC(i)} = \frac{d_{TPC}(t_{i+1}) - d_{TPC}(t_i)}{(t_{i+1} - t_i)} \quad (1)$$

where $d_{TPC}(t_{i+1})$ and $d_{TPC}(t_i)$ were TPC line diameters measured for two subsequent frames from the recorded movies. The time step ($t_{i+1} - t_i$) in the case of water was 0.0625 ms, while in SDS solutions, due to slower expansion of TPC line, was equal to 0.25 ms.

Experiments were performed at 25 °C in pure water and in an aqueous solution of the anionic surfactant sodium dodecyl sulphate (SDS) at concentration $2 \times 10^{-2} \text{ mol} \cdot \text{dm}^{-3}$. This concentration is above the critical micelle concentration equal to $8 \times 10^{-3} \text{ mol} \cdot \text{dm}^{-3}$. SDS was purchased from Sigma-Aldrich Chemical Company (for ion pair chromatography, details in Basarova et al., 2017) and used as received. The surface tension of water at 25°C was $72.4 \text{ mN} \cdot \text{m}^{-1}$. In case of SDS, we measured the dynamic surface tension using the Krüss tenziometer BP100 employing the maximum bubble pressure method. After 1 second, we observed the equilibrium and the surface tension was $38.5 \text{ mN} \cdot \text{m}^{-1}$.

2.2. Numerical calculations

To reproduce experimental conditions, phenomena occurring during bubble attachment to the hydrophobic solid wall immersed in liquid phase was calculated numerically by solving the governing equations, describing the conservation of momentum and mass of an incompressible, viscous liquid in the form (Popinet, 2009):

$$\rho \left(\frac{\partial \mathbf{u}}{\partial t} + \mathbf{u} \cdot \nabla \mathbf{u} \right) = -\nabla p + \nabla \cdot (2\mu \mathbf{Q}) + \sigma \kappa \delta_s \mathbf{n} \quad (2)$$

$$\nabla \cdot \mathbf{u} = 0 \quad (3)$$

using spatial discretization and numerical scheme described in details in (Popinet, 2003; Popinet, 2009; Fuster et al., 2009), where \mathbf{Q} is a deformation tensor defined as:

$$\mathbf{Q} = \frac{1}{2} (\nabla \mathbf{u} + (\mathbf{u})^T) \quad (4)$$

while $\mathbf{u} = [u_x, u_r]$ is the fluid velocity vector, ρ is the density and μ is the viscosity of the fluid, p is a pressure, t is time, σ is surface tension, δ_s is a Dirac distribution function (expressing the fact that the surface tension term is concentrated at the interface), while κ and \mathbf{n} are the curvature and normal unit vector to the interface, respectively.

Fig. 1 presents scheme of the computational domain. The calculations were performed using a two-dimensional, axi-symmetrical, cylindrical coordinate system. Radius of the computational domain (L) was equal to 2 mm. A spherical bubble of diameter $d_b = 2r_b$ (adjusted according to the experiment) was placed beneath the horizontal, no-slip, solid wall. Slip boundary conditions were assumed at the bottom, left and right boundaries to minimize the wall effects. For all computational domain walls, Dirichlet boundary conditions were applied. The computational domain was spatially discretized using square finite volumes called cells, which were hierarchically organized as *quadtree* (Popinet, 2003). An adaptive refinement algorithm (AMR) was applied to adjust the spatial discretization to follow the scale and temporal evolution of the flow structures. Such an approach implies that the computational mesh size varies in the domain. The grid size depends on refinement level and is directly related to the L value (Popinet, 2003; Zawala, 2016). The AMR implies also that the finest grid cell can be found at the liquid/gas interface and in its vicinity. In our calculations, for $L = 2$ mm and refinement level equal to 9, the smallest grid cell was equal to $3.9 \mu\text{m}$. As was shown elsewhere (Zawala, 2016) for $L = 2$ mm this refinement level is enough for computational results convergence.

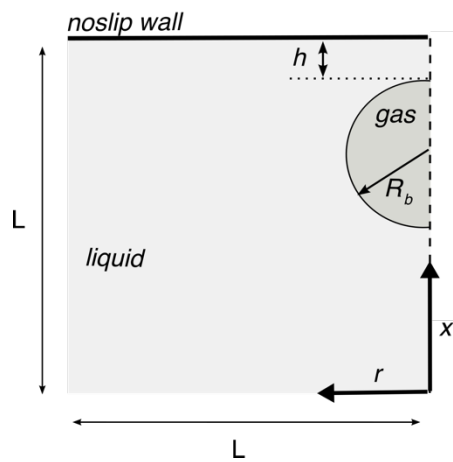


Fig. 1. Scheme of the computational domain

The distance of the bubble top apex to the solid/liquid interface, i.e. initial thickness of the liquid film (h), was set to be equal to $35 \mu\text{m}$. This thickness resulted from numerical reasons - a bubble has to be located at the distance equal to several computational cells from the solid/liquid interface to assure stability of calculations. The density of the liquid and gas were 1000 and 1.3 kg/m^3 , respectively, i.e. equal to density of water and air. Similarly, the dynamic viscosity of liquid and gas was taken as 1×10^{-3} and $18 \times 10^{-6} \text{ Pa}\cdot\text{s}$, respectively. Similar to experimental conditions, the surface tension was assumed to be equal $72.4 \text{ mN}\cdot\text{m}^{-1}$. The contact angle of the solid surface depended on the level of refinement of the solid boundary (Afkhami et al. 2009) and, under chosen computational conditions, was around 80° for bubble with fully mobile interface. To take into account bubble surface immobilization by the presence of surfactant adsorption layer, the original volume of fluid algorithm was modified. Keeping all other physicochemical parameters of the system constant, different viscosity value at the liquid/bubble interface (surface viscosity), implying secondary tangential stresses near the interface, were used in

calculations. This approach simulated bubble surface fluidity retardation in surface-active substance solution of high concentration (Zawala et al. 2016). The total kinetic energy of the system was calculated using the formula (Zawala 2016):

$$T = \frac{1}{2} \int 2\pi r \rho u \, dx \, dr \quad (5)$$

3. Results and discussion

3.1. Experimental determination of the TPC line spreading kinetics in pure water and surfactant solutions

Fig. 2 shows the bubble adhesion ($d_b = 0.705$ mm) to the hydrophobic solid surface in pure water. The first image at $t = 0$ ms illustrates the situation just before the film rupture. The bubble sits at the solid surface practically motionless, after complete dissipation of its kinetic energy, related to bouncing and associated shape oscillations. The initial zero time is set as the time of the rupture of the liquid interface film and it was set on the basis of visual observation together with the calculated change of d_{TPC} . The formation of the three-phase contact line is visible after 0.0625 seconds (camera time step) on the second shot. The TPC line expansion continues together with significant bubble shape deformation, where the bubble vertical diameter is firstly extended and then compressed. While the diameter of the three-phase contact line does not change significantly anymore, the bubble shape deformation is still observable. The bubble shape deformation during expansion could be described as a form of bouncing while keeping the three-phase contact (liquid/gas interface pulsates). The images illustrate the bubble adhesion process during the first three milliseconds. Even after this time there were visible some oscillations, but the shape of the bubble did not change too much. The whole sequence consists of 5000 images including collision process and final equilibrium.

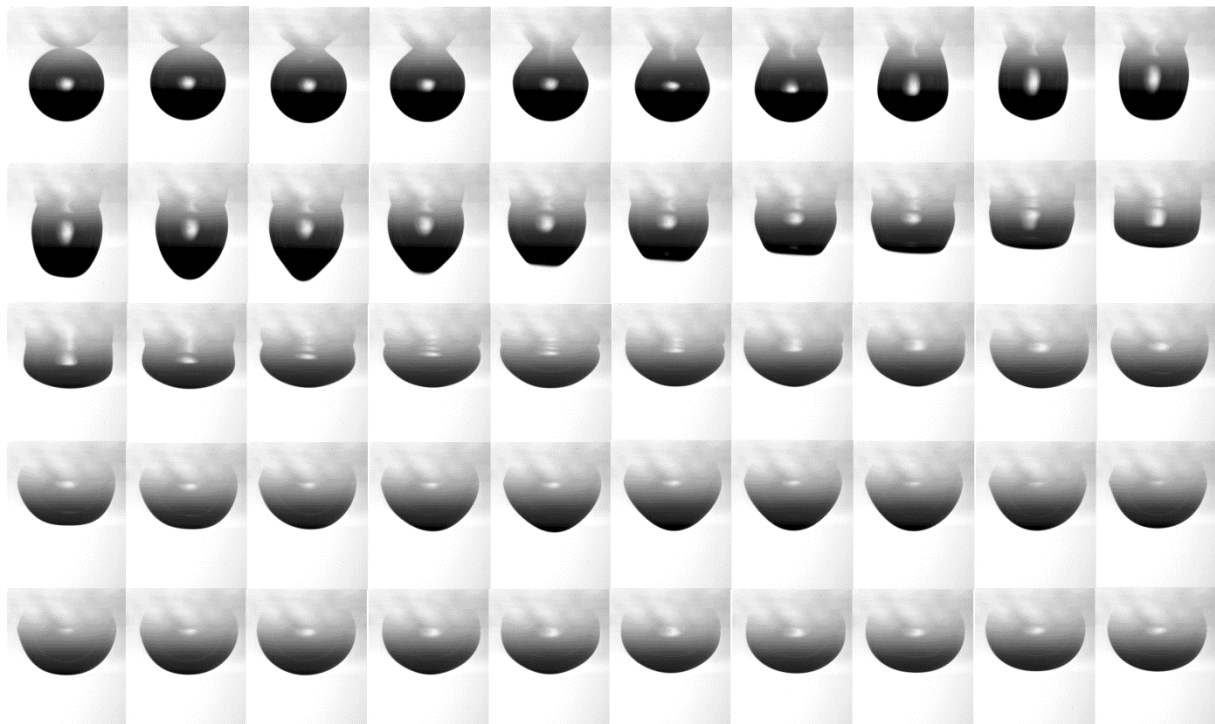


Fig. 2. A series of photos illustrating the adhesion of the bubble ($d_b = 0.705$ mm) onto the hydrophobic solid surface in pure water. The time interval between individual shots is 0.0625 ms

The bubble adhesion illustrated above can be characterised quantitatively using variations in diameter of the TPC line (d_{TPC}), velocity of the TPC line expansion (U_{TPC}) and the position of the bubble bottom coordinate (y_{bottom}). Fig. 3 presents the data which were calculated for the bubble adhesion process presented in Fig. 2. The bubble diameter (before liquid film rupture – first photo in Fig. 2) is

0.705 mm and the time step between individual images is 0.0625 milliseconds. We observed bubble flattening due to buoyancy before the formation of TPC line and thus y_{bottom} (at $t=0$ ms) is smaller than d_b . The non-zero value of d_{TPC} at $t = 0$ ms does not have a physical meaning and it is a result of computer data processing – this is the diameter of liquid film (contact between bubble and solid surface) just before its rupture. The TPC line expands very quickly; the velocity reaches its maximum in the first captured moment (0.1 ms). The TPC line continues to expand but with a decreasing velocity. At around 1.3 ms the expansion velocity increases again and unexpected second peak can be observed with its maximum at $t = 1.4$ ms. On the d_{TPC} curve, one can see that this effect is associated with a small S-shape course. After that, the TPC line diameter reaches a stable value and the expansion velocity becomes zero. This whole process from TPC line formation to stable TPC position took 1.7 ms. Even though the bubble shape continues to change after this point (see left image in Fig. 3) it does not affect the length of TPC line significantly anymore. Also the contact angle does not change. The equilibrium contact angle in this case was 99.5° . To conclude, during the first 2 ms after liquid film rupture we can observe quick TPC line expansion connected with the change of bubble shape. Fig. 3 shows also the change of the bubble bottom apex position (y_{bottom}) in the vertical direction over time. In first 0.5 milliseconds, no change was observed even though both d_{TPC} and U_{TPC} change dramatically. During the quick bubble adhesion part the bottom apex position decreases significantly due to the bubble flattening. After that, we can observe typical oscillations. The period between the individual peaks is 1.2 ms and the whole process is muted after 20 ms.

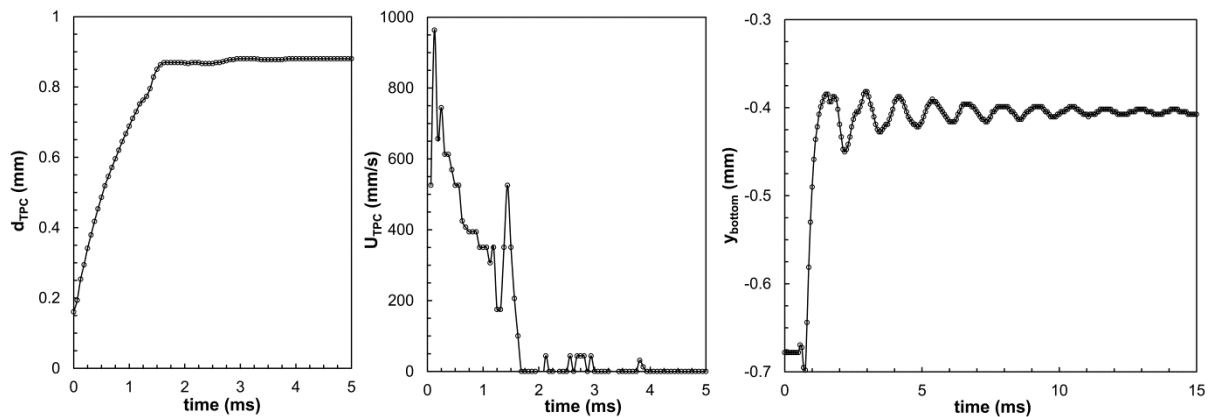


Fig. 3. The time dependence of the diameter of the TPC line (left), TPC expansion velocity (middle) and bubble bottom apex position (right) in pure water for a bubble with diameter 0.705. The time interval between individual points is 0.0625 ms

Fig. 4 shows the TPC diameter and expansion velocity for two different bubble sizes in water. The points represent the average value measured from 3-4 sequences. The courses of the two monitored quantities are similar. The TPC diameter increases with bubble size. The ratio d_{TPC}/d_b remains constant as the wetting angle does not change. The average value of the contact angle was $97.8^\circ \pm 2.2^\circ$. Although it seems that the bubble size does not significantly influence the extent of the velocity, it significantly influences the timing. The smaller the bubble, the earlier the velocity peak appears and the earlier the equilibrium diameter (zero velocity) is reached. To conclude, typical features of bubble adhesion in pure water are i) fast TPC line expansion (finished in 2 ms), ii) bubble shape deformation during the adhesion, iii) additional maximum on velocity profile and iv) bubble shape oscillations.

The second part of experiments was done in aqueous solution of the surface-active agent SDS. The concentration is $2 \times 10^{-2} \text{ mol} \cdot \text{l}^{-1}$ which is above the critical micelle concentration. Under these conditions we assume a fully immobile surface of the bubble. Fig. 5 illustrates the bubble adhesion process ($d_b = 0.712$ mm) onto the hydrophobic surface in a solution of SDS. The first image at $t = 0$ ms illustrates the situation just before the liquid film rupture. The camera captured a bubble motion with a time step of 0.0625 milliseconds. However, images with a 0.25 millisecond time step are shown in the Fig. 5. Expansion of the TPC line is very slow and small differences are not perceived by the human eye. The bubble shape changes, particularly the oscillations in vertical direction like in pure water, were not

detected. The TPC line expansion continues together with bubble shape change, but the bubble keeps the spherical shape. The images illustrate the bubble adhesion process during the first ten milliseconds. Even after this time there are visible some small changes but the shape of the bubble does not change. The equilibrium state is reached after 50 ms. The whole sequence consists of 5400 images including final equilibrium. The bubble rising and its collision with the solid surface was not captured because the time lapse between the collision and the actual formation of the TPC line was longer than is possible to capture. Also, no bubble bouncing was observed. The extended time of the liquid interface film depletion is caused by the high concentration of surfactant molecules, which stabilises the interface film (Malysa et al., 2005).

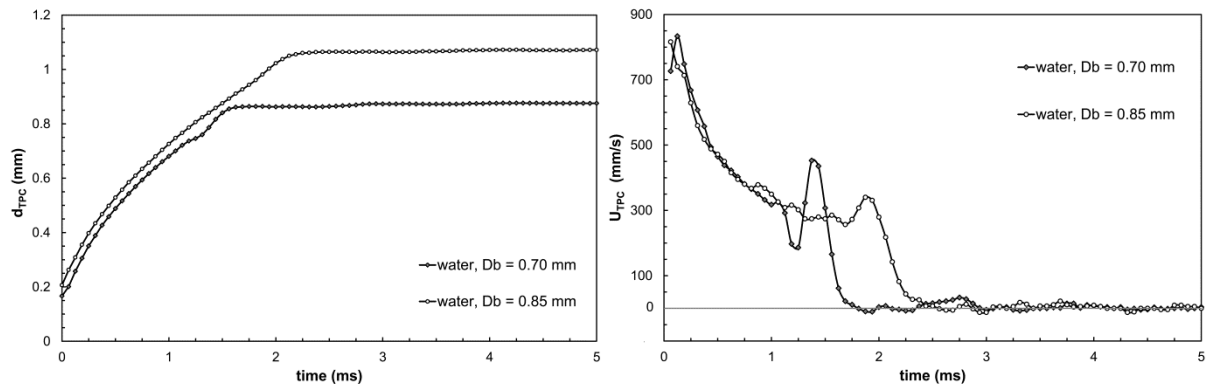


Fig. 4. The average data of diameter of the TPC line and TPC expansion velocity in pure water for bubbles with diameters 0.70 mm and 0.85 mm. The time interval between individual points is 0.0625 ms

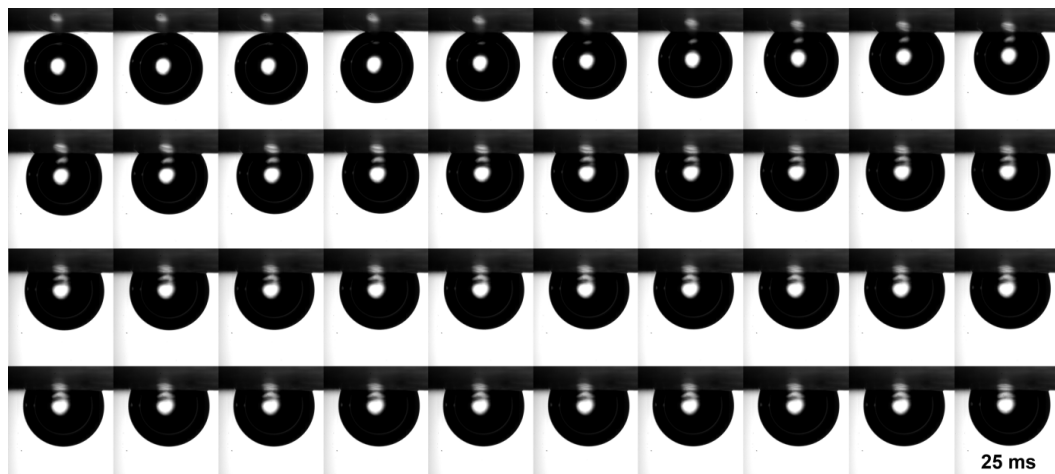


Fig. 5. Sequence of photos illustrating a course and outcome of the bubble ($d_b = 0.712$ mm) adhesion onto the solid surface in aqueous solution of SDS. The time interval between individual points is 0.25 ms. The final image represents equilibrium at $t = 25$ ms

Calculated data for this sequence, namely d_{TPC} , U_{TPC} and y_{bottom} , are given in Fig. 6. Note different time range when compared with Fig. 3. The diameter of the TPC line increases very slowly without any oscillations and the equilibrium was observed after 50 milliseconds. The bubble keeps the spherical shape and the equilibrium contact angle is 69.5° . The velocity of TPC expansion is captured in the middle image. We use the time step 0.5 ms for this calculation. The data was captured at 16000 fps but the change of d_{TPC} distance did not differ much from the calibration length. Therefore, a longer period of time was used. The chart clearly shows first the increase in U_{TPC} , where the maximum is reached after 3 millisecond. Then the velocity decreases and acquires almost unmeasurable values after 25

milliseconds. The velocity of TPC expansion in surfactant solution is at least ten times slower than in water. The last graph shows the movement of the bubble bottom apex in vertical direction. The movement of the lower part of the bubble was detected after 0.5 ms after the liquid film rupture. The bubble oscillations are completely muted during the bubble adhesion and the bottom position was stable after 12 ms.

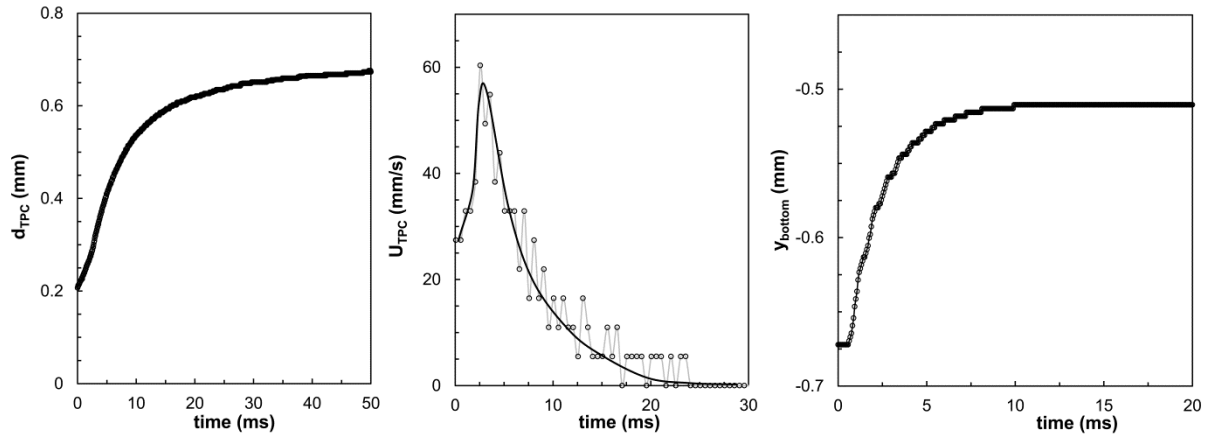


Fig. 6. The time dependence of the diameter of the TPC line (left), TPC expansion velocity (middle) and bubble bottom apex position (right) in SDS solution for a bubble with diameter 0.712 mm

Fig. 7 shows the TPC diameter and expansion velocity for two different bubble sizes in SDS solution. The points represent the average value measured from 4-5 sequences. The TPC diameter increases with bubble size. The ratio d_{TPC}/d_b remains constant again and the average value of the contact angle is $69.4^\circ \pm 1.7^\circ$. The velocity of TPC expansion is completely different in solutions of surface active agents when compared with pure water. The velocity is much slower and we can observe an initial increase of U_{TPC} after 3 milliseconds. The times coordinate of the maximum increases with bubble size. After reaching this maximum, the velocity slowly decreases. The large scattering of data is caused by a small difference of the input data. To conclude, typical features of bubble adhesion in solutions of surface active agents are i) slow TPC line expansion (finished after 20 ms), ii) no bubble shape deformation during the adhesion, and iii) a maximum on velocity profile after 3 ms.

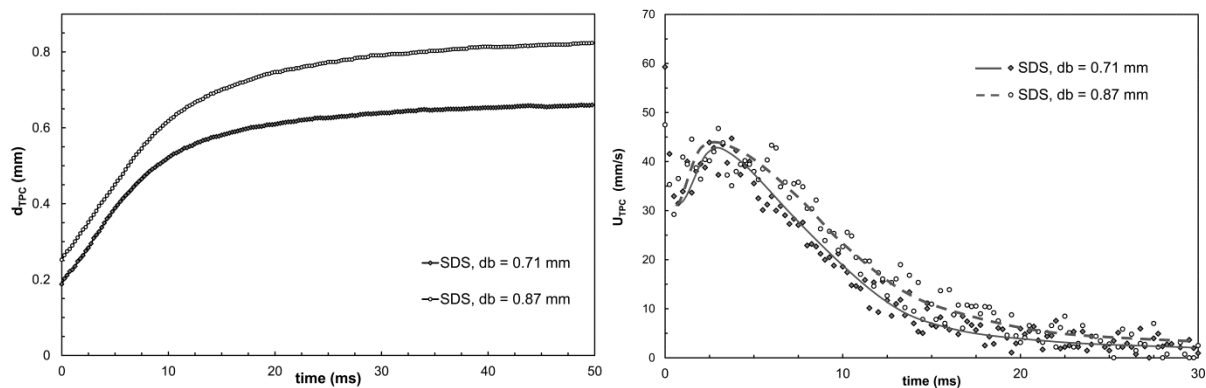


Fig. 7. The average data of diameter of the TPC line and TPC expansion velocity in SDS solution for bubbles with diameters 0.71 mm and 0.87 mm. The time interval between individual points is 0.25 ms

2.3. Simulations of the TPC line spreading

2.3.1 Mobile liquid/gas interface (water)

Fig. 8 presents simulation snapshots illustrating calculated outline of the bubble during (i) resting at solid surface ($t < 0$), rupture of the intervening liquid film ($t = 0$), formation of TPC hole ($t = 0.1$ ms) and TPC line spreading ($t > 0.1$ ms) for completely mobile liquid/gas interface (i.e. for situation

corresponding to distilled water). Corresponding time values are marked at each snapshot. Note, that similar to the experimental case presented in Fig. 2, also here characteristic elongation of the bubble shape, associated with the TPC formation and spreading can be noticed (see pictures for $t = 0.4$ and 0.7 ms). Moreover, bubble is flattened after elongation period ($t = 1.2$ ms), what is also consistent with experimental observations.

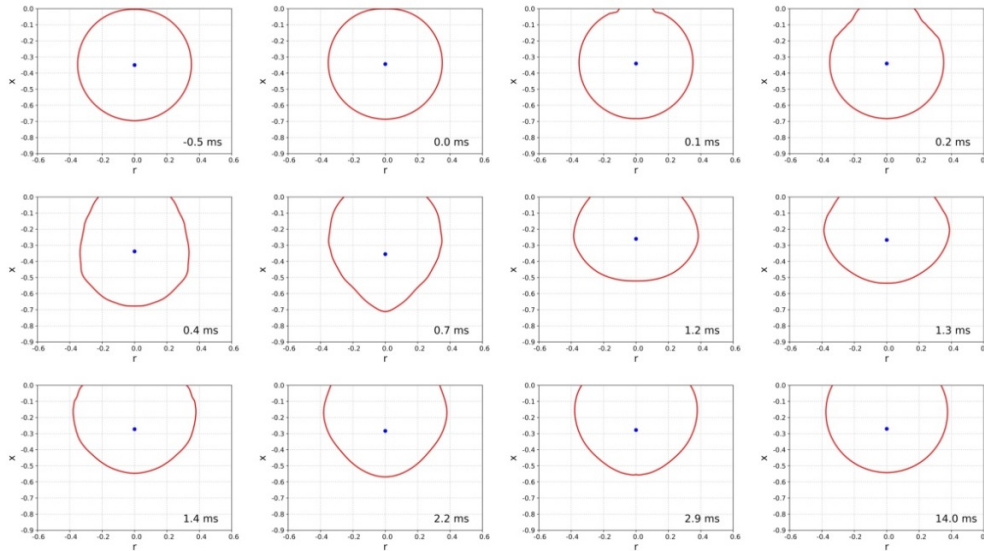


Fig. 8. Chosen simulation snapshots illustrating calculated bubble shapes during wetting film rupture and TPC line spreading

Evolutions of the TPC line diameter as well as the TPC line expansion velocity obtained in numerical simulations for d_b values corresponding to those studied experimentally (0.70 and 0.85 mm), are presented in Fig. 9. These dependencies look quite similar (qualitatively and quantitatively) to experimental data presented in Fig. 4, confirming quite a nice agreement between experimental observation and numerical simulation results. Characteristic peaks for the TPC expansion velocity around 1 – 2 ms after the wetting film rupture are clearly visible. Initially the velocity of TPC line spreading is comparable for both d_b values and ca. 1.5 ms first maximum for smaller bubble appears. The second maximum of U_{TPC} for larger bubble is shifted towards higher time values. Comparing the bubble shape variations observed in Fig. 8 with U_{TPC} variations presented in Fig. 9 (Fig. 2 and 4 in the case of experiment, respectively) it seems that the velocity peak is associated with the most violent bubble shape variations, i.e. with the situation, when, after the TPC formation, the bubble shape is first elongated and then flattened (the change in the bubble bottom pole position is relatively big and equal to ca. 0.2 mm). The elongation of the bubble shape results from interplay between detachment and attachment forces (Kosior and Zawala 2017). Due to the TPC formation, the capillary force (related to diameter of the TPC perimeter) is too strong for the bubble for its detachment. Consequently, the bubble is pushed back (see for example pictures for $t = 1.2 - 1.3$ ms in Fig. 8), what is most probable source of additional pressing force (additional pressure), facilitating (speeding up) the rate of expansion of the TPC line (maximum at U_{TPC} vs time curves).

This hypothesis impose that characteristic peaks observed at U_{TPC} vs time curves (Fig. 4 and 9) has only hydrodynamic origin and is associated with local increase of total kinetic energy of the system, resulting from quite violent bubble shape pulsations. To check correctness of this claim - thanks to the numerical simulations - we can look a little bit deeper into to the nature of this effect, analysing quantities, which are impossible to obtain experimentally. Fig. 10 presents comparison between variations in the position of bubble bottom apex (for $d_b = 0.70$ mm) and calculated kinetic energy of the system (kinetic energy of the liquid which motion is induced by the bubble shape variations). Again, $t = 0$ means rupture of the wetting film and TPC formation. As seen, initially the kinetic energy is constant and just after the moment of TPC hole formation and expansion increases significantly. Simultaneously, the bubble bottom pole approaches much closer to the solid surface - this change is quite significant

and occurs in fraction of millisecond, only. Then, small changes in the y_{bottom} and the T can be noticed, followed by relatively large peak (both for y_{bottom} and T) for t equal to ca. 1.5 ms. This is exactly this same t value for which maximum at U_{TPC} vs time curve can be observed (see Fig. 4 and 9 for $d_b = 0.70$ mm). Existence of this T peak, which is a consequence of quite violent bubble shape variations (manifested by y_{bottom} changes) proves correctness of explanation of above-mentioned mechanism and explains nature of characteristic and unexpected maxima at U_{TPC} vs time curves.

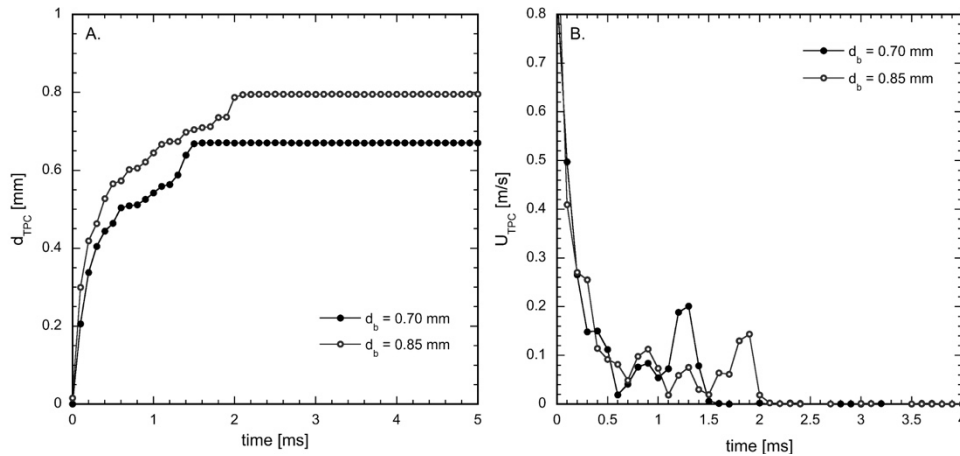


Fig. 9. Variations in: (A) diameter of the TPC line and (B) velocity of the TPC line spreading as a function of time for two different bubble sizes and mobile liquid/gas interface)

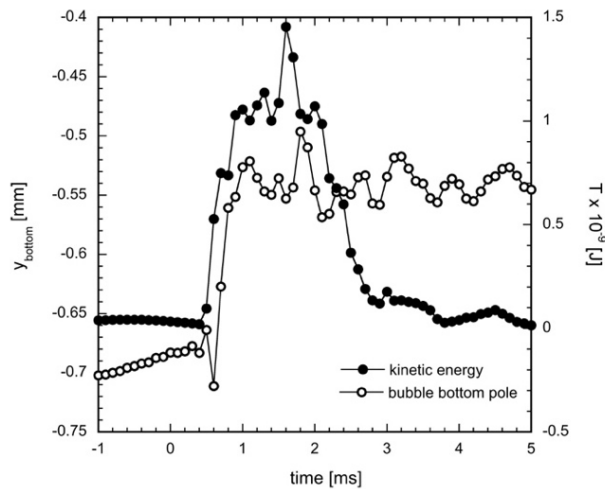


Fig. 10. Variations in position of the bubble bottom apex (solid surface positioned at $y = 0$) and total kinetic energy of the system during liquid film rupture ($t = 0$) and TPC line expansion for bubble of $d_b = 0.70$ mm (mobile liquid/gas interface)

The TPC line expansion in pure systems is influenced mainly by hydrodynamics. Such explanation is valid for smooth hydrophobic solid surface. It is possible that TPC line expansion can be influenced also by higher roughness, presence of air entrapped in the surface grooves and cavities, non-uniform chemical composition of the solid surface, different degree of hydrophobicity etc. In our system, however, we believe that hydrodynamic factor is a key parameter determining TPC line expansion course.

2.3.1 Immobilized liquid/gas interface (solution of surface-active substance)

To explain big difference between kinetics of the TPC line expansion in solution of surface-active substance and in pure water observed experimentally (see Figs. 6-7), variations in y_{bottom} of the bubble just before and after TPC hole formation was compared in Fig. 11A. To visualize strong influence of

degree of liquid/gas interface mobility, the y_{bottom} changes during TPC line expansion were presented there for a bubble with fully mobile (slip) and fully immobilized (no-slip) interface. As seen, fully mobile interface was much more deformable (as already discussed above) what resulted in quite violent changes in bubble bottom apex position. In contrast, due to liquid/gas interface immobilization (rigidity), which in real experimental conditions is caused by presence of surfactant and its adsorption at the bubble surface, bubble shape pulsations are significantly damped.

Certainly, as a consequence, totally different course of kinetic energy variations in the system can be observed. Due to significant attenuation of the bubble shape pulsations for immobilized liquid/gas interface, kinetic energy changes were much smaller and smoother. This explains difference in d_{TPC} and U_{TPC} evolution observed in distilled water and SDS solution determined on the basis of experimental data.

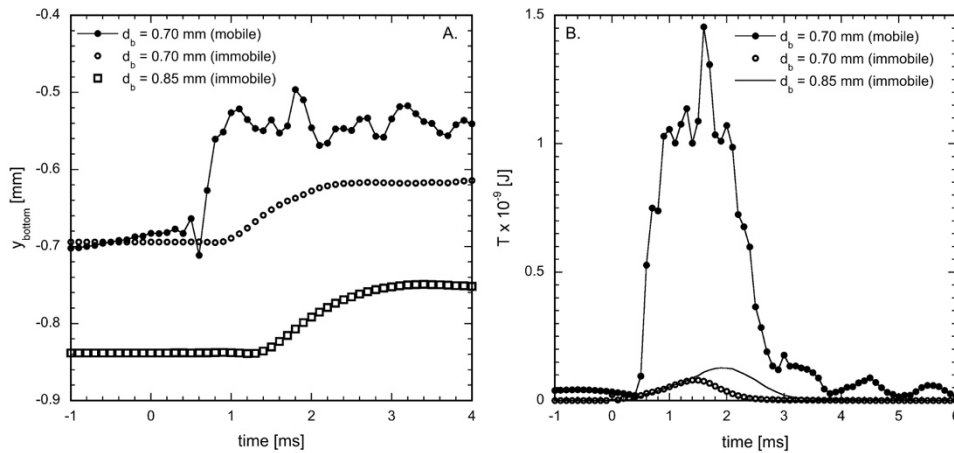


Fig. 11. Variations in: (A) position of the bubble bottom apex (solid surface positioned at $y = 0$) and (B) total kinetic energy of the system during liquid film rupture and TPC line expansion for bubble of two different size (mobile and immobile liquid/gas interface)

Fig. 12 presents evolution of the d_{TPC} (normalized to d_b) for mobile and immobilized bubble surface. The lack of characteristic S-shape course, already discussed in the experimental section, is clearly noticeable here for immobilized liquid/gas interface. Despite quite similar courses of expansion of the TPC line diameter determined experimentally and numerically, we were not able, unfortunately, to accurately reproduced the velocity of the TPC line spreading. Numerically determined velocity is presented in Fig. 12B (compare with Fig. 7).

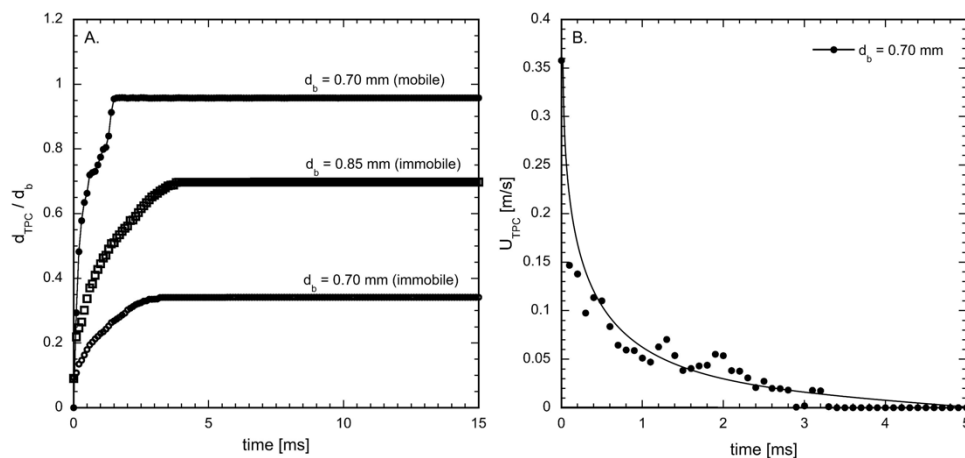


Fig. 12. Time evolution of (A) normalized TPC diameter and (B) TPC line spreading velocity (numerical results)

The reason of the main (long and smooth) peak observed for surfactant solution is probably connected with the existence of the gradient of surface tension. The bubble stays under the surface for up to tens of seconds without any change or motion. During this period, the liquid thin film very slowly thins and surfactant molecules spread all over the bubble surface. After creating the TPC line we should consider also the interfacial gradient of surface tension and concentration of molecules (the reverse Marangoni flow). The bubble surface area decreases and thus the surface concentration increases. The initial increase of velocity may be related to the surface tension gradient, which was not taken into account in numerical simulations. As was already discussed, model used to mimic presence of adsorption layer at the bubble surface was simple and assumed global immobilization of the liquid/gas interface only by viscous drag increase.

3. Conclusions

The kinetics of the TPC line expansion during bubble collision and rupture at hydrophobic solid surface is significantly influenced by the bubble shape oscillations, which are diminished in case of surfactant presence.

In case of completely mobile liquid/gas interface, corresponding to pure water, characteristic bubble shape oscillations were observed during the TPC line formation and expansion. The TPC expansion velocity vs time curve exhibits a characteristic peak around 1 – 2 ms after the liquid film rupture. We proved that this characteristic peak has the hydrodynamic origin and is associated with local increase of total kinetic energy of the system, resulting from quite violent bubble shape pulsations.

In surfactant solutions, the effect of the liquid/gas interface immobilization is very significant, because the bubble shape pulsations are damped and kinetic energy changes were much smaller and smoother. The forces of surface tension gradient overcome the viscous forces and the hydrodynamic model is not able to explain the non-monotonic curve of the expansion velocity profile in surfactant solutions.

Acknowledgments

Authors would like to acknowledge the financial support from specific university research fund of the Ministry of Education, Youth and Sport of the Czech Republic No 20-SVV/2017.

References

- AFKHAMI, S., ZALESKI, S., BUSSMANN, M., 2009. *A mesh-dependent model for applying dynamic contact angles to VOF simulations*. J. Comput. Phys. 228, 5370–5389.
- BASAROVA, P., SUCHANOVA, H., SOUSKOVA, K., VACHOVA, T., 2017. *Bubble adhesion on hydrophobic surfaces in solutions of pure and technical grade ionic surfactants*. Colloid Surf. A 522, 485–493.
- BASAROVA, P., SOUSKOVA, K., 2018. *Detailed experimental study of bubble adhesion on hydrophobic surface*. Physicochem. Probl. Miner. Process. 54(1), 111–123.
- BLAKE T.D., HAYNES, J.M., 1969. *Kinetics of Liquid/Liquid Displacement*, J Colloid Interf Sci, 30, 421–423.
- COX R.G., 1986. *The Dynamics of the Spreading of Liquids on a Solid-Surface .1. Viscous-Flow*, J Fluid Mech, 168, 169–194.
- FUSTER, D., AGBAGLAH, G., JOSSERAND, C., POPINET, S., ZALESKI, S., 2009. *Numerical simulation of droplets, bubbles and waves: state of the art*, Fluid Dyn. Res. 41, 065001.
- HUBICKA, M., BASAROVA, P., VEJRAZKA, J., 2013. *Collision of a small rising bubble with a large falling particle*, Int. J. Miner. Process. 121, 21–30.
- HUH C., SCRIVEN, L.E., 1971. *Hydrodynamic Model of Steady Movement of a Solid/Liquid/Fluid Contact Line*, J Colloid Interf. Sci, 35, 85–101.
- KOSIOR, D., ZAWALA, J., KRASOWSKA, M., MALYSA, K. 2013. *Influence of n-octanol and alpha-terpineol on thin film stability and bubble attachment to hydrophobic surface*, Phys. Chem. Chem. Phys. 15, 2586–2595.
- KRASOWSKA, M., ZAWALA, J., MALYSA, K., 2009. *Air at hydrophobic surfaces and kinetics of three phase contact formation*, Adv Colloid Interfac, 147–48, 155–169.
- NGUYEN, A.V., SCHULZE H.J., RALSTON J., 1997. *Elementary steps in particle-bubble attachment*, Int. J Miner. Process. 51, 183–195.

- POPINET, S., 2003. *Gerris: a tree-based adaptive solver for the incompressible Euler equations in complex geometries*, J. Comput. Phys. 190, 572-600.
- POPINET, S., 2009. *An accurate adaptive solver for surface-tension-driven interfacial flows*. J. Comput. Phys. 228, 5838-5866.
- RADULOVIC, J., SEFIANE, K., STAROV, V.M., IVANOVA, N.S. 2013. *Review on Kinetics of Spreading and Wetting by Aqueous Surfactant Solutions*, in: M.L. Ferrari, L. Miller, R. (Ed.) *Drops and Bubbles in Contact with Solid Surfaces*, CRC Press, Boca Raton, 2013.
- RANABOTHU, S. R., KARNEZIS, C., DAL, L. L. 2005. *Dynamic wetting: Hydrodynamic or molecular-kinetic?* J. Colloid Interface Sci. 288, 213-221.
- VOBECKA, L., VEJRAZKA, J., TIHON, J., 2013. *Modification of shape oscillations of an attached bubble by surfactants*. EPJ Web of conferences 45, 01095.
- YARNOLD, G.D.M., MASON, B.J., 1949. *Theory of the Angle of Contact*, Proc. Phys. Soc. B, 62, 121-125.
- ZAWALA, J., KOSIOR, D., MALYSA, K., 2015. *Formation and influence of the dynamic adsorption layer on kinetics of the rising bubble collisions with solution/gas and solution/solid interfaces*, Adv Colloid Interfac, 222, 765-778.
- ZAWALA, J., 2016. *Energy balance in viscous liquid containing a bubble: rise due to buoyancy*. Can. J. Chem. Eng., 94, 586-595.
- ZAWALA, J., KOSIOR, D., 2016. *Dynamics of dewetting and bubble attachment to rough hydrophobic surfaces - measurements and modelling*, Minerals. Eng. 85, 112-122.